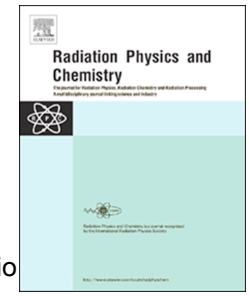

Gamma rays induced synthesis of graphene oxide/gold nanoparticle composites: Structural and photothermal study

Dejan P. Kepić, Andjela M. Stefanović, Milica D. Budimir, Vladimir B. Pavlović, Aurelio Bonasera, Michelangelo Scopelliti, Biljana M. Todorović Marković

PII: S0969-806X(22)00581-3

DOI: https://doi.org/10.1016/j.radphyschem.2022.110545

Reference: RPC 110545

To appear in: *Radiation Physics and Chemistry*

Received Date: 25 July 2022

Revised Date: 9 September 2022

Accepted Date: 13 September 2022

Please cite this article as: Kepić, D.P., Stefanović, A.M., Budimir, M.D., Pavlović, V.B., Bonasera, A., Scopelliti, M., Todorović Marković, B.M., Gamma rays induced synthesis of graphene oxide/gold nanoparticle composites: Structural and photothermal study, *Radiation Physics and Chemistry* (2022), doi: https://doi.org/10.1016/j.radphyschem.2022.110545.

D.P. Kepić: Conceptualization, Writing - Original Draft, Visualization. **A.M. Stefanović:** Investigation. **M.D. Budimir:** Resources, Writing - Review & Editing. **V.B. Pavlović:** Resources. **A. Bonasera:** Resources. **M. Scopelliti:** Resources. **B.M. Todorović-Marković:** Supervision, Project administration, Funding acquisition.

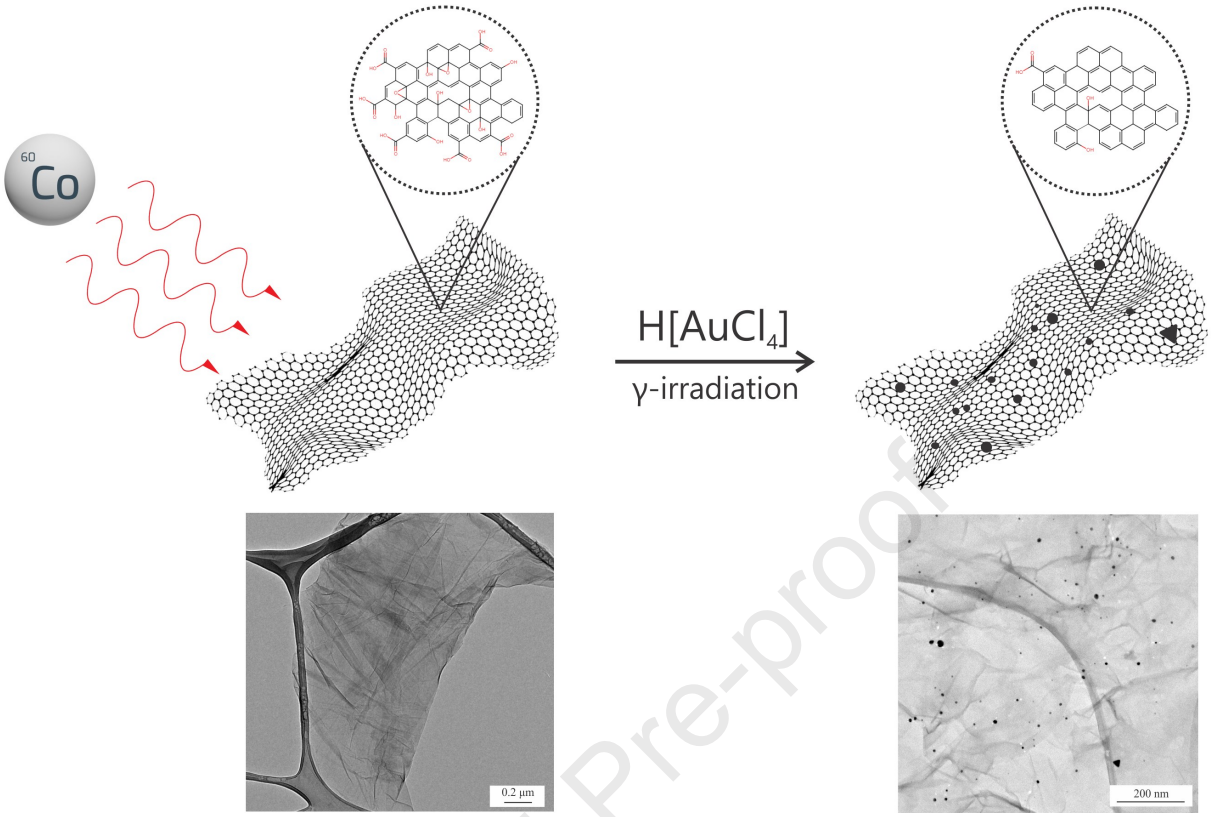

Gamma rays induced synthesis of graphene oxide/gold nanoparticle composites: structural and photothermal study

Dejan P. Kepić[1*], Andjela M. Stefanović[1,2], Milica D. Budimir[1], Vladimir B. Pavlović[3], Aurelio Bonasera[4], Michelangelo Scopelliti[4], Biljana M. Todorović Marković[1]

[1]Vinča Institute of Nuclear Sciences - National Institute of the Republic of Serbia, University of Belgrade, P.O.B. 522, 11001 Belgrade, Serbia

[2]Faculty of Chemistry, University of Belgrade, Studentski trg 12-16, 11158 Belgrade, Serbia

[3]Faculty of Agriculture, Department of Agricultural Engineering, University of Belgrade, Nemanjina 6, 11080 Belgrade, Serbia

[4]Department of Physics and Chemistry - Emilio Segrè, University of Palermo and Consorzio Interuniversitario Nazionale per la Scienza e Tecnologia dei Materiali (INSTM), Palermo Research Unit, Viale delle Scienze, Bdg. 17, 90128 Palermo, Italy

[*]Corresponding author. E-mail address: d.kepic@vin.bg.ac.rs

Keywords: Graphene oxide, Gold nanoparticles, Gamma irradiation, One-step synthesis, Photothermal properties

Abstract

Gamma irradiation provides an alternative pathway to conventional gold nanoparticle synthesis because it is simple, fast, and economical. Here, we employed gamma irradiation at low doses (1-20 kGy) to obtain gold nanoparticles (Au NPs) anchored onto graphene oxide (GO) sheets. GO was selected as a suitable platform for the nucleation and growth of Au NPs because of its large surface area and good dispersibility in water due to the presence of polar oxygen-containing functional groups in its structure. Gamma irradiation at all the applied doses led to the reduction of chloroauric acid and the formation of evenly distributed Au NPs at the GO surface, simultaneously causing the reduction of GO and partial restoration of the graphene structure. As-prepared Au NPs have predominately spheric shapes and the smallest nanoparticles were reported for the dose of 1 kGy. The increase in the irradiation dose caused either the growth of larger particles (5 and 10 kGy) or the broad distribution of particles' sizes (20 kGy). All samples showed a temperature increase upon exposure to 800 nm laser and photothermal efficiency was the highest for the sample prepared at 20 kGy.

1. Introduction

Graphene is a material composed of a single-atom layer of sp^2 hybridized carbon atoms arranged in a hexagonal honeycomb structure. It is often labeled as a wonder material for the future due to its excellent and unique properties [1, 2]. Being lightweight, highly flexible, ultra-thin, elastic, and an excellent conductor of heat and electricity, graphene paves its way to many applications

that stretch from the field of electronics, sensors, energy storage, new materials, and protective coatings to biomedicine, catalysis, and environmental applications [3, 4]. To make it dispersible in water, graphene is covalently modified by strong oxidants to introduce oxygen functional groups and obtain graphene oxide (GO) [5]. In the structure of GO, hydroxyl and epoxy groups are attached to sp^3 hybridized carbon atoms on the basal plane of GO, while carboxyl and carbonyl groups are located at the edges of sheets attached to sp^2 hybridized carbon atoms [6]. However, the chemical modification of graphene negatively affects its electrical conductivity because it disrupts its conjugated structure [7]. For specific applications it is required to restore graphene's conjugated structure by reduction which could be conducted chemically, thermally, electrochemically, or hydrothermally, to mention some [8].

It was calculated that single-layer graphene has a surface area close to 2600 $m^2 g^{-1}$ [9], which makes graphene and GO excellent platforms for the *in situ* growth of various species, including polymer chains [10] and metallic nanoparticles (NPs) [11, 12], to create novel composite materials with synergistic properties. It was found that oxygen-bearing functionalities from the surface of GO could act as reactive sites for the spontaneous chemical reduction of Ag^+ ions, thus playing an important role in the nucleation and growth of silver NPs [13]. Besides, growing the NPs directly on graphene sheets prevents their agglomeration and overgrowth which makes the use of an additional stabilizing agent redundant [14]. Graphene decorated with metallic NPs finds numerous applications, such as sensors [15, 16], catalysts [17], surface-enhanced Raman scattering (SERS) platforms [13, 18], and photothermal agents [14, 19]. Photothermal therapy of cancer exploits the effect of the selective hyperthermia of tumorous tissue. Firstly, the photothermally active species are delivered into the tumorous tissue. After that, the irradiation from the near-infrared or therapeutic window is applied and the absorbed light is converted into heat which irreversibly damages the tumorous tissue while the healthy surrounding tissue remains unaffected. Nanoparticles of gold (Au NPs) showed great potential to be applied as photothermal agents due to their ability to convert the absorbed light into heat [20-22]. An additional advantage of Au NPs is the possibility to tune their optical properties by modifying their dimensions and structure [19].

The most common method for Au NPs synthesis involves the reduction of chloroauric acid by sodium citrate at an elevated temperature [23]. Besides, Au NPs were prepared by the reduction of chloroauric acid under UV light exposure in the presence of either various surfactants [24] or polymer medium [25] used to stabilize the freshly formed Au NPs. Alternatively, Au NPs could be obtained by employing gamma irradiation [14, 26]. Gamma irradiation does not require elevated temperatures and additional reductants, therefore providing a fast and economical strategy for Au NPs production. To date, it has been employed to obtain several graphene-based composites with different metallic NPs [27-31]. In this paper, we employed gamma irradiation at low doses (1-20 kGy) to obtain Au NPs anchored onto GO sheets in a one-step synthetic procedure. The obtained GO/Au NPs composites were analyzed by different microscopy and spectroscopy characterization methods with a special emphasis on their morphological and

structural changes induced by gamma irradiation. The photothermal properties of the composites were determined by measuring the temperature changes under an 800 nm laser exposure.

2. Experimental

2.1. Sample preparation

GO was prepared according to a modified Hummers' method from pure graphite powder. Briefly, a mixture of concentrated H_2SO_4 (46 ml, Carlo Erba Reagents), $NaNO_3$ (1 g, Lach-Ner), and graphite powder (2 g, Sigma-Aldrich) was firstly cooled down to 0 °C in an ice bath. Then, $KMnO_4$ was added (6 g, Merck) under continuous stirring in a water bath maintaining the temperature of the solution below 20 °C. After 30 minutes the temperature of the reaction mixture was firstly elevated to 35 °C, after which the distilled water (100 ml) was added and the temperature was raised to 98 °C and kept for 2 h. After that time the reaction mixture was diluted with 400 ml of water and 30% H_2O_2 (2 ml, Macron Fine Chemicals) was added and left to cool down to room temperature. The synthesized GO was purified by repeated washing with distilled water and centrifugation until the pH of the supernatant was neutral. Finally, the water was evaporated and GO dried in the oven at 60 °C overnight.

GO powder (180 mg) was dispersed in 180 ml of deionized MilliQ water using an ultrasound bath. In the dispersion, chloroauric acid (4.5 mg, Sigma-Aldrich) and isopropyl alcohol (8 ml, Fisher Chemical) were added and well homogenized. The mixture was then transferred to vials and purged with argon for 15 min to remove dissolved oxygen, after which the vials were hermetically sealed. Samples were exposed to the gamma irradiation source (^{60}Co nuclide, dose rate of 9 kGy/h) absorbing the doses of 1, 5, 10, and 20 kGy. After the irradiation, samples were filtered (0.2 μm pore size, Isopore Membrane Filters), washed with deionized water, and dried in the oven at 60 °C.

2.2. Sample characterization

Transmission electron microscopy (TEM) analyses were performed on TEM-JEOL JEM-1400 microscope operated at an accelerating voltage of 120 kV. The samples were dispersed in ethanol using an ultrasound bath and a drop of dispersion was deposited on lacey carbon copper grids (200 mesh) and dried in air. Gwyddion software version 2.44 was used to determine the particle size distributions.

Scanning electron microscopy (SEM) analyses were performed on JEOL JSM-6390LV (Tokyo, Japan) microscope at room temperature. Powder samples were fixed on carbon adhesive tape. EDS measurements were performed on Oxford Instruments Aztec X-max (Abingdon, UK) energy dispersive spectroscope.

The UV-Vis absorption spectra were recorded using LLG-uniSPEC 2 spectrophotometer. For the measurements, a small amount of dried sample was dispersed in water, and spectra were recorded in quartz cuvettes at room temperature.

Fourier transform infrared spectroscopy (FTIR) spectra were recorded using Avatar 370 Thermo Nicolet spectrometer. A small amount of each sample was mixed with KBr and recorded in a form of a pellet.

X-ray Photoelectron Spectroscopy (XPS) analysis spectra were obtained using a PHI5000 VersaProbe II scanning microprobe (ULVAC-PHI, Inc.; Chigasaki, Japan), operating with a monochromatic Al Kα source (1486.6 eV). Used X-Ray beam had ⌀ 100 μm (25 W, 15 kV); low-resolution surveys were collected using pass energy (PE) of 117.000 eV, with a resolution of 1.0 eV; high-resolution scans were collected with a PE of 23.500 eV, with a resolution of 0.05 eV. Collected electrons were analyzed in FAT mode. A few drops of sample dispersed in ethanol were placed onto freshly cleaned alumina substrates and dried in air; during the data acquisition the sample surface was kept at an angle of 45° with respect to the analyzer; charge neutralization was used during all the experiments by means of both electrons and positive ions (Ar^+).

2.3. Determination of photothermal properties

Samples were homogeneously dispersed in 2 ml of deionized water using an ultrasound bath to obtain GO/Au NPs concentrations of 1 mg/ml. The dispersions were exposed to 800 nm Mai Tai NIR laser radiation (Spectra Physics, Santa Clara, CA, USA) in a Petri dish at room temperature (21.0 °C) (Figure 1). The laser irradiance was 1.65 W/cm^2. The temperature of the samples was monitored at the laser irradiation spot every 10 s by a thermo-vision camera (FLIR, E40, Wilsonville, OR, USA) using the supporting analysis software (± 0.1 °C accuracy). After 10 min of laser irradiation, the laser was switched off and the samples were left to cool down for another 10 min during which the temperature drop was monitored.

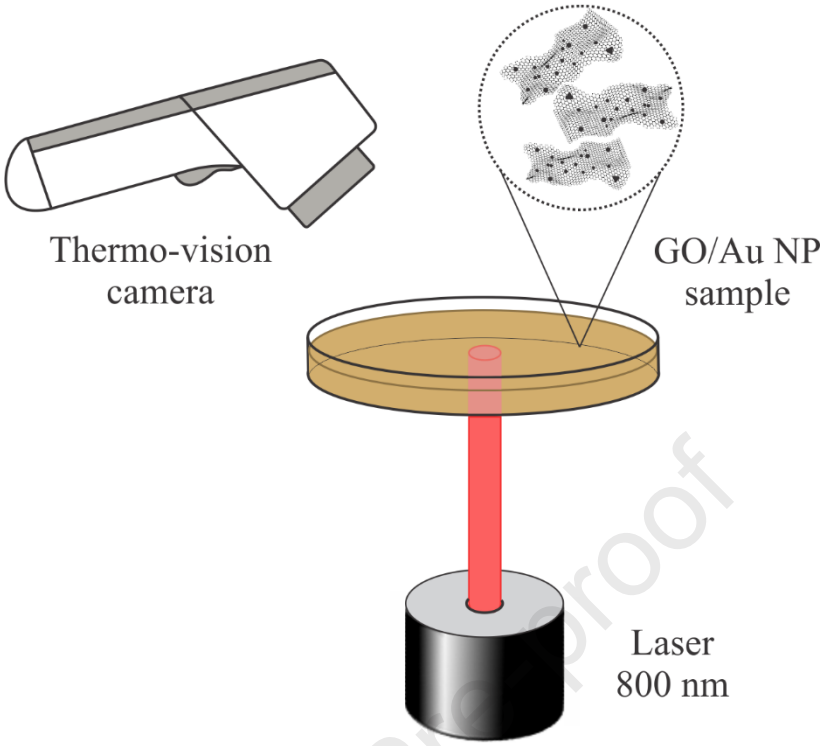

Figure 1. An illustration of the experimental setup for the determination of photothermal properties of GO/Au NP composites.

The photothermal efficiency (η) of the samples was calculated using Roper's method according to the equation:

$$\eta = \frac{hS(T_{max} - T_{amb}) - Q_{loss}}{I(1 - 10^{-A_{800}})} \quad (1)$$

where h represents the heat transfer coefficient, S the surface area of the irradiated sample, and T_{max} and T_{amb} are the maximum and the ambient temperature, respectively. I represents the laser power, A_{800} the absorbance of the samples at 800 nm, and Q_{loss} is the heat dissipated from the light absorbed by the solvent and the cuvette. The value hS was calculated according to the equation:

$$hS = \frac{m_{water}\, C_{water} + m_{sample}\, C_{sample}}{\tau_s} \quad (2)$$

where m_{water} and m_{sample} are the mass of the water and GO/Au NP composite, and C_{water} and C_{sample} are the specific heat capacity of water and GO/Au NP composite, respectively. τ_s is the time constant that was calculated from Figure 7b using the equations:

$$\theta = \frac{T - T_{amb}}{T_{max} - T_{amb}} \quad (3)$$

and

$$t = -\tau_s \ln(\theta) \quad (4)$$

3. Results and discussion

Graphene-supported gold nanoparticles were synthesized via the reduction of chloroauric acid under gamma irradiation at low doses. Gamma-ray photons from ^{60}Co as a source have energies of 1.173 and 1.332 MeV which is sufficient to induce a breakdown of water molecules and form reactive species such as $e^-_{(aq)}$, $H^\bullet$, $OH^\bullet$, OH^-, H_3O^+, H_2, H_2O_2, etc. These species are classified either as reductive ($e^-_{(aq)}$, $H^\bullet$), oxidative ($OH^\bullet$, H_2O_2), or inert species (H_2). The introduction of a scavenger of oxidative species, such as secondary alcohols, suppresses the influence of oxidative species and creates an exclusively reductive environment. Additionally, before the irradiation, an inert gas was bubbled through the reaction mixture to remove dissolved oxygen. In this way, the predominant are the effects of strong reductants $e^-_{(aq)}$ and $H^\bullet$ with standard potentials of -2.9 V/SHE and -2.4 V/SHE, respectively [32].

Reductive species formed during the radiolysis of water in the presence of isopropyl alcohol induce the reduction of $[AuCl_4]^-$ ions to Au^0. Parallel to this, the radiolysis also causes the reduction of GO which was evidenced by the gradual color change of the GO dispersion from dark brownish to black as the irradiation dose increases. The structural changes of GO induced by gamma irradiation were monitored by UV-vis spectroscopy (Figure 2). The spectrum of non-irradiated GO has two distinct features: one dominant peak at ~230 nm that originates from π-π* transition of aromatic C=C bonds, and a shoulder at about 300 nm that stems from n-π* transition of C=O bonds [33]. The peak at ~230 nm shows a gradual redshift with the increase of the irradiation dose, while the shoulder at 300 nm decreases until its total disappearance at the higher applied doses of 10 and 20 kGy. This indicates the partial restoration of graphene's conjugated structure upon reduction and the elimination of oxygen-bearing functionalities [34, 35]. The localized surface plasmon resonance peak of Au NPs at 530 nm is greatly suppressed due to the low initial concentration of $[AuCl_4]^-$ ions and could not be observed.

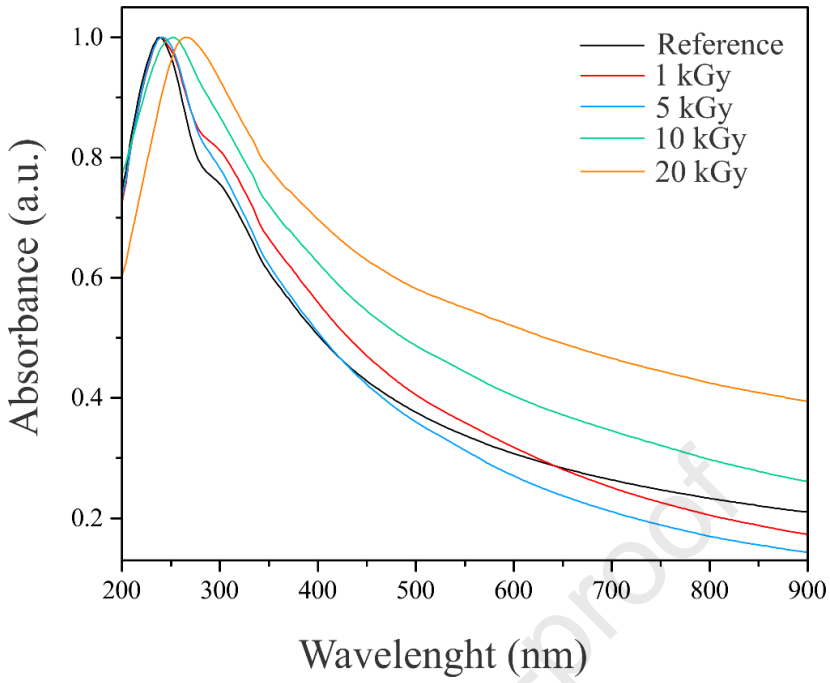

Figure 2. Normalized UV-vis spectra of GO (reference) and GO/Au NP composites obtained at different irradiation doses.

FTIR spectra (Figure 3) confirm the reduction of GO upon irradiation. All spectra show one broad band at 3400-3500 cm^{-1} originating from the stretching mode of hydroxyl groups, bands at 2925 and 2855 cm^{-1} from C-H vibrations, and bands at 1725 cm^{-1}, 1185 cm^{-1}, 1625 cm^{-1} and 1390 cm^{-1} that stem from C=O and C-O stretching vibrations and O-H and C-H bending vibrations, respectively [36]. With the increase in the irradiation dose, the bands at 1725 cm^{-1} and 1185 cm^{-1} become less prominent and almost completely vanish for the sample irradiated at 20 kGy. Additionally, the band at 1625 cm^{-1} shows a lower intensity with the increase of the absorbed dose. In the spectra of the sample irradiated at 20 kGy a small intensity band at ~1570 cm^{-1} can be detected that originates from C=C stretching vibrations.

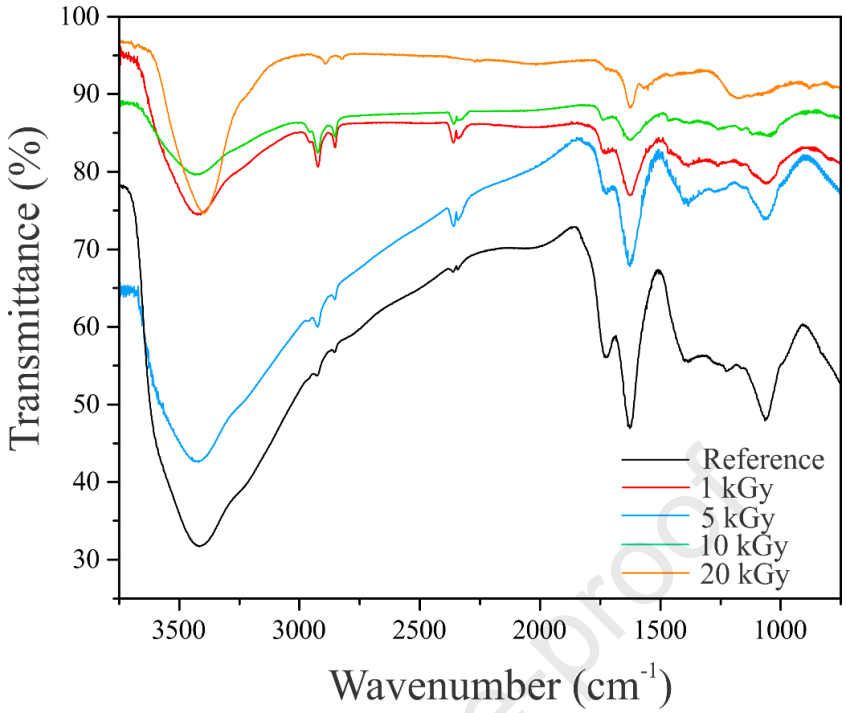

Figure 3. FTIR spectra of GO (reference) and GO/Au NP composites obtained at different irradiation doses.

The deconvolution of the high-resolution XPS spectra over the C1s area further confirmed the decreased oxidation degree and the increased graphitic carbon contribution as the irradiation dose increased. The deconvoluted C1s XPS spectra showed the features at 284.5 eV, 286.6 eV, and ~288.5 eV that correspond to graphitic carbon, carboxylic (O-C=O), and oxide (C-O) functional groups, respectively [37]. As can be seen from Figure 4 and Table 1, the relative abundances of carboxylic and oxide functional groups gradually decreased from 5.83% and 32.24% for GO to 1.09% and 9.60%, respectively, for the sample prepared at the highest applied dose (20 kGy).

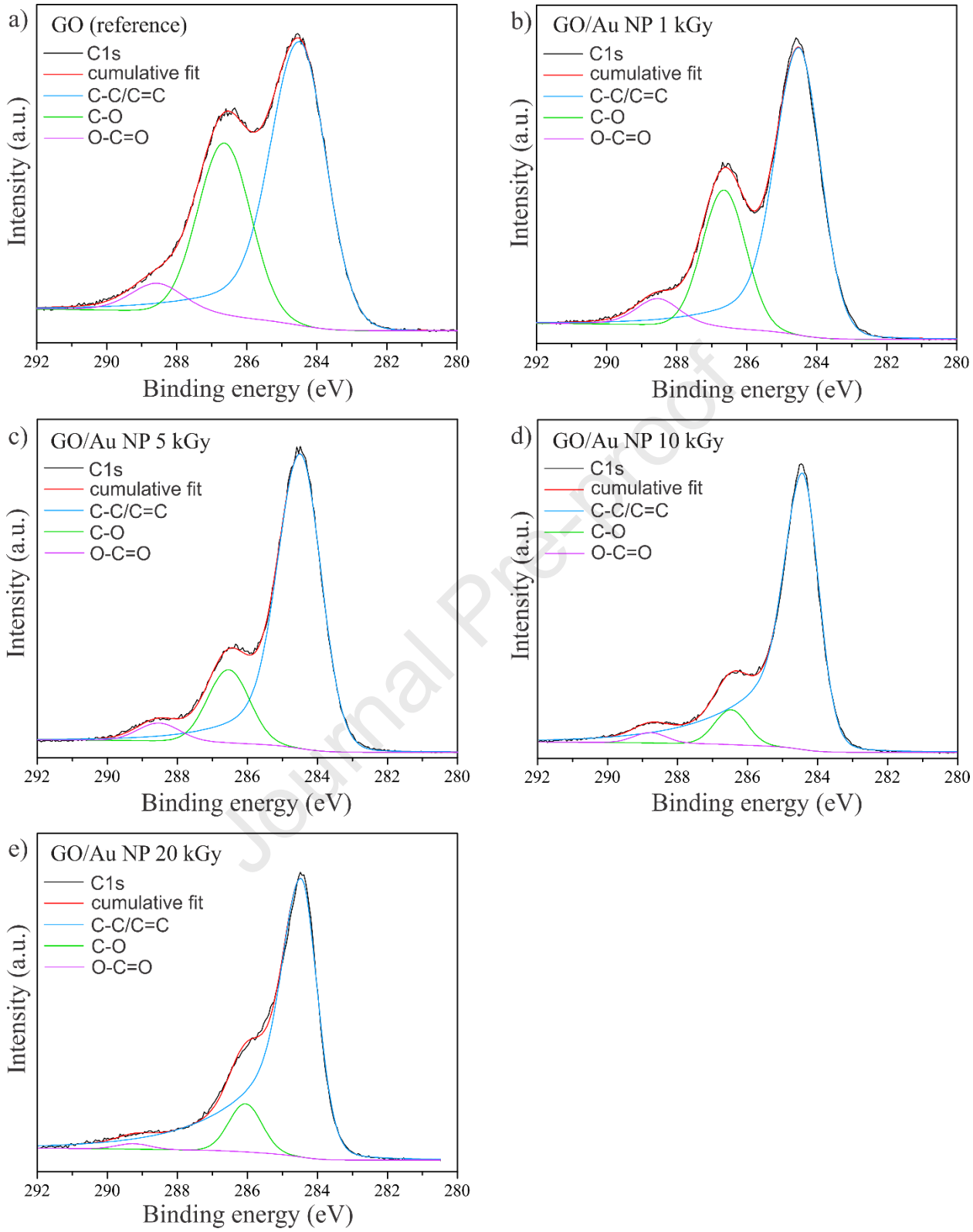

Figure 4. Deconvoluted XPS spectra of GO (a) and GO/Au NP composites obtained at different irradiation doses (b-e).

Table 1. The relative abundances of characteristic components from deconvoluted C1s peak.

Sample	Attribution	Value (eV)	Relative abundance (%)
GO (reference)	Graphitic	284.50	61.93
	Oxide	286.65	32.24
	Carboxylic	288.58	5.83
GO/Au NP 1 kGy	Graphitic	284.50	67.23
	Oxide	286.63	26.97
	Carboxylic	288.53	5.81
GO/Au NP 5 kGy	Graphitic	284.50	79.33
	Oxide	286.54	16.62
	Carboxylic	288.54	4.05
GO/Au NP 10 kGy	Graphitic	284.50	90.23
	Oxide	286.52	7.54
	Carboxylic	288.83	2.23
GO/Au NP 20 kGy	Graphitic	284.50	89.31
	Oxide	286.08	9.60
	Carboxylic	289.28	1.09

SEM-EDS analyses were performed for samples of pristine GO and GO/Au NP composites obtained at the lowest and the highest applied dose (1 and 20 kGy, respectively, Figure 5). For the pristine GO, carbon and oxygen atoms were detected with traces amount of sulfur remaining from the synthesis by the Hummers' method. Oxygen atoms homogeneously cover the graphene surface and the O/C weight ratio is 0.54. GO/Au NP composites prepared at 1 and 20 kGy also show the homogenous distribution of oxygen over the graphene surface and the homogeneous coverage of graphene by gold nanoparticles. The O/C weight ratio for the sample prepared at 1 kGy is similar to pristine GO (0.53), while for the sample prepared at 20 kGy is comparably smaller (0.22) which is an additional confirmation of the partial reduction of GO caused by the irradiation.

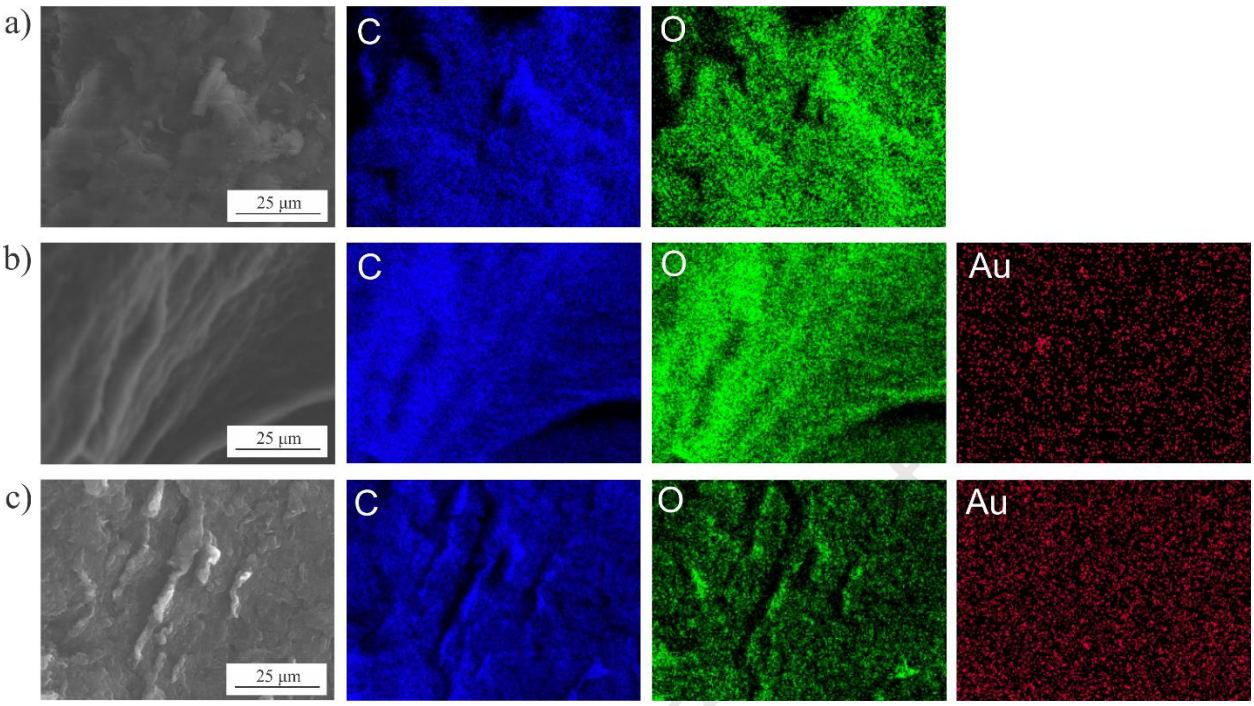

Figure 5. SEM image and EDS maps of the corresponding area for carbon, oxygen, and gold for a) pristine GO, b) GO/Au NP composite prepared at 1 kGy irradiation dose, and c) GO/Au NP composite prepared at 20 kGy irradiation dose.

TEM analysis was employed to estimate GO morphology and the size and shape of Au NPs (Figure 6). TEM images of the GO sample reveal the presence of both single and few-layer graphene with a wrinkled surface and folded edges. The average GO sheet sizes are up to several micrometers. After the irradiation, the GO surface is homogeneously covered with Au NPs and no significant changes in GO sheet sizes or morphology were observed for all the applied doses. Au NPs have a predominately spherical shape and only a negligible portion of nanoparticles have triangular or irregular shape morphology. Au NPs prepared at the dose of 1 kGy have sizes of up to 20 nm and the majority of nanoparticles are smaller than 10 nm. With the increase in the irradiation dose, the obtained Au NPs are larger and their sizes are between 30 and 110 nm. For the highest applied dose of 20 kGy a wide range of Au NPs sizes was detected ranging from several nanometers to 120 nm.

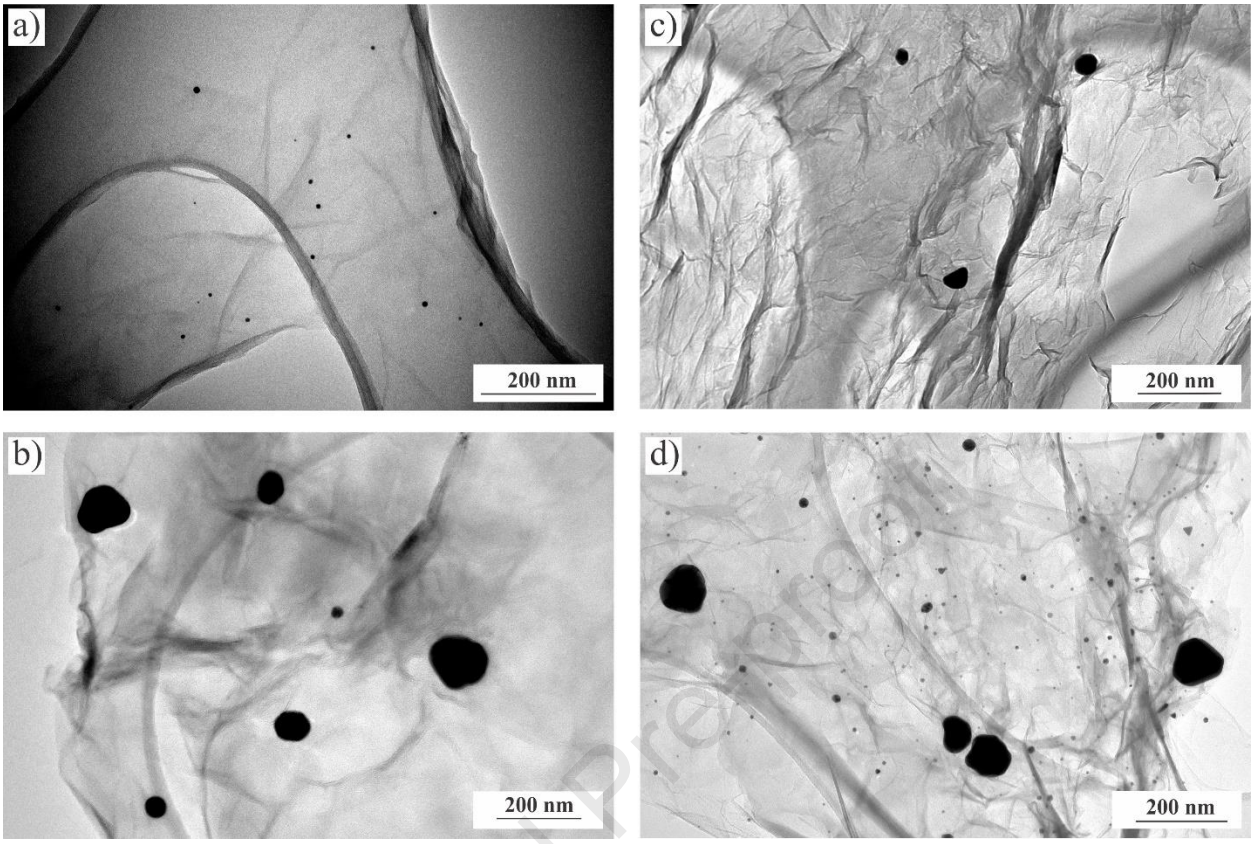

Figure 6. TEM images of GO/Au NP composites prepared at a) 1 kGy irradiation dose, b) 5 kGy irradiation dose, c) 10 kGy irradiation dose, and d) 20 kGy irradiation dose.

Photothermal efficiency of GO/Au NP samples was estimated by monitoring the temperature changes induced by laser irradiation. Samples were irradiated by an 800 nm laser for 10 minutes after which the laser was switched off and the temperature decrease was monitored for an additional 10 minutes in 10-second intervals. The temperature changes for GO/Au NP samples dispersed in water are shown in Figure 7a.

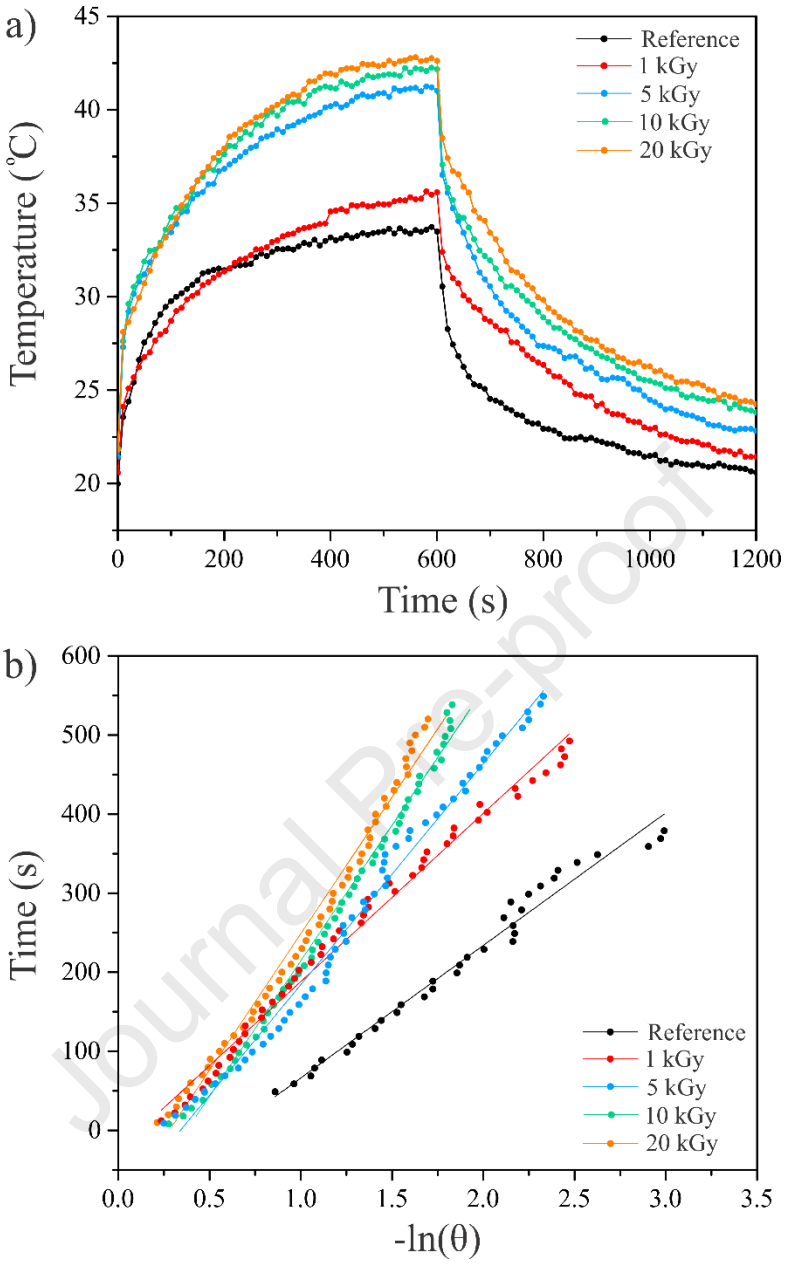

Figure 7. a) The temperature changes of GO (reference) and GO/Au NP samples prepared at different irradiation doses, and b) linear fit of time data versus -ln(θ).

The laser irradiation of pure water did not cause an increase in the temperature even for the prolonged time interval. On the other hand, pristine GO and all the GO/Au NP samples show temperature elevation upon laser irradiation. As expected, the lowest temperature elevation (12.5 °C) was observed for the pristine GO sample, and as the gamma irradiation dose increases the rise in the temperature becomes higher with the highest value of 21.6 °C for the GO/Au NP sample prepared at 20 kGy. The photothermal efficiency (η) of the samples was calculated using Roper's method by measuring the temperature decrease data when the laser was switched off

[38, 39]. By taking into account the τ_s values obtained from the data presented in Figure 7b and calculated according to the equations (3) and (4), *hS* values calculated according to the equation (2), laser incident power of 1.3 W, absorbances of samples at 800 nm (Figure 1), the photothermal efficiency was calculated according to the equation (1). As it can be seen from Table 2, the highest photothermal efficiency has the GO/Au NP sample prepared at 20 kGy, and with the decrease of the gamma irradiation dose, the photothermal efficiency becomes comparably smaller.

Table 2. Photothermal efficiency calculations for GO sample (reference) and GO/Au NP samples obtained at different irradiation doses.

Sample	Temperature elevation °C	Time constant τ_s	Absorbance A_{800} nm	Photothermal efficiency η
GO (reference)	12.5	167.65	0.14	13.59%
GO/Au NP 1 kGy	14.6	212.76	0.12	14.40%
GO/Au NP 5 kGy	20.0	279.52	0.13	14.24%
GO/Au NP 10 kGy	21.2	342.74	0.11	14.23%
GO/Au NP 20 kGy	21.6	345.18	0.10	15.71%

The ability of Au NPs to convert the absorbed light into heat is due to the localized surface plasmon resonance (LSPR) effect, which involves the oscillations of the surface electrons at the Au NPs. Therefore, the photothermal efficiency is determined by the surface area of the material i.e. the size and shape of NPs. For example, Yang et al. found the highest photothermal conversion efficiency for Au nanostars because due to their multiple branches they have a larger surface area compared to nanospheres and nanorods [40]. Jiang et al. reported the increased light-to-heat energy conversion efficiency with the decrease of Au NPs size [41]. On the other hand, delocalized p-electrons in graphene sp^2 lattice are also capable to convert incident light into thermal energy and transfer it to the surrounding medium [42]. Compared to GO, graphene has higher photothermal efficiency [43]. This behavior is due to the isolated sp^2 domains in the GO structure which become partially restored with the removal of oxygen functional groups upon reduction [44]. Hence, the observed increase in the calculated photothermal efficiency of GO/Au NP composites with the increase of the irradiation dose could be attributed to the combination of two factors: the change in Au NPs sizes and the reduction of GO caused by gamma radiation.

4. Conclusion

Gold nanoparticles (Au NPs) anchored onto graphene oxide (GO) sheets were prepared by the reduction of chloroauric acid under low-dose gamma irradiation (1-20 kGy) in a one-step process. The large surface area of graphene presents an excellent platform for the nucleation and growth of freshly-formed Au NPs, simultaneously preventing their agglomeration. The prepared

Au NPs have predominately spherical shapes and are homogeneously distributed at the GO surface. The smallest Au NPs were prepared by employing the irradiation dose of 1 kGy. The increase in the irradiation dose caused either the growth of larger particles (5 and 10 kGy) or the broad distribution of particles' sizes (20 kGy). Simultaneously, gamma irradiation in an exclusively reductive environment leads to the partial restoration of graphene's conjugated structure and to some extent the elimination of oxygen-bearing functionalities. The prepared GO/Au NP composites dispersed in water were exposed to an 800 nm laser irradiance and the temperature increase upon exposure was observed for all the samples. Calculated photothermal efficiency showed an increasing trend with the increase of the irradiation dose, which could be attributed to both the change in the size of Au NPs and the reduction of GO caused by gamma radiation.

Acknowledgment

The research was supported by the Science Fund of the Republic of Serbia, #7741955, Are photoactive nanoparticles salvation for global inflectional treath? - PHOTOGUN4MICROBES and by the Ministry of Education, Science and Technological Development of the Republic of Serbia, grant number 451-03-68/2022-14/200017. The authors acknowledge generous help and useful advice from Giuseppe Chirico, Laura D'Alfonso, and Maddalena Collini from the Department of Physics, University of Milano-Bicocca, Milan, Italy. M. Budimir acknowledges the financial support of the Ministry of Education, Science and Technological Development of the Republic of Serbia for postdoctoral research.

References

[1] M. Chakraborty, M.S.J. Hashmi, Wonder material graphene: properties, synthesis and practical applications, Advances in Materials and Processing Technologies, 4 (2018) 573-602.
[2] J.R. Prekodravac, D.P. Kepić, J.C. Colmenares, D.A. Giannakoudakis, S.P. Jovanović, A comprehensive review on selected graphene synthesis methods: from electrochemical exfoliation through rapid thermal annealing towards biomass pyrolysis, Journal of Materials Chemistry C, 9 (2021) 6722-6748.
[3] V. Dhinakaran, M. Lavanya, K. Vigneswari, M. Ravichandran, M.D. Vijayakumar, Review on exploration of graphene in diverse applications and its future horizon, Materials Today: Proceedings, 27 (2020) 824-828.
[4] M.A. Al Faruque, M. Syduzzaman, J. Sarkar, K. Bilisik, M. Naebe, A Review on the Production Methods and Applications of Graphene-Based Materials, Nanomaterials, 11 (2021) 2414.
[5] W.S. Hummers, R.E. Offeman, Preparation of Graphitic Oxide, Journal of the American Chemical Society, 80 (1958) 1339-1339.
[6] V. Singh, D. Joung, L. Zhai, S. Das, S.I. Khondaker, S. Seal, Graphene based materials: Past, present and future, Progress in Materials Science, 56 (2011) 1178-1271.
[7] S. Rao, J. Upadhyay, K. Polychronopoulou, R. Umer, R. Das, Reduced Graphene Oxide: Effect of Reduction on Electrical Conductivity, Journal of Composites Science, 2 (2018) 25.

[8] V. Agarwal, P.B. Zetterlund, Strategies for reduction of graphene oxide – A comprehensive review, Chemical Engineering Journal, 405 (2021) 127018.
[9] A. Ghosh, K.S. Subrahmanyam, K.S. Krishna, S. Datta, A. Govindaraj, S.K. Pati, C.N.R. Rao, Uptake of H2 and CO2 by Graphene, The Journal of Physical Chemistry C, 112 (2008) 15704-15707.
[10] K. Mylvaganam, L. Zhang, In Situ Polymerization on Graphene Surfaces, The Journal of Physical Chemistry C, 117 (2013) 2817-2823.
[11] X. Zhou, X. Huang, X. Qi, S. Wu, C. Xue, F.Y.C. Boey, Q. Yan, P. Chen, H. Zhang, In Situ Synthesis of Metal Nanoparticles on Single-Layer Graphene Oxide and Reduced Graphene Oxide Surfaces, The Journal of Physical Chemistry C, 113 (2009) 10842-10846.
[12] L.-N. Zhang, H.-H. Deng, F.-L. Lin, X.-W. Xu, S.-H. Weng, A.-L. Liu, X.-H. Lin, X.-H. Xia, W. Chen, In Situ Growth of Porous Platinum Nanoparticles on Graphene Oxide for Colorimetric Detection of Cancer Cells, Analytical Chemistry, 86 (2014) 2711-2718.
[13] K. Spilarewicz-Stanek, A. Kisielewska, J. Ginter, K. Bałuszyńska, I. Piwoński, Elucidation of the function of oxygen moieties on graphene oxide and reduced graphene oxide in the nucleation and growth of silver nanoparticles, RSC Advances, 6 (2016) 60056-60067.
[14] D.P. Kepić, D.N. Kleut, Z.M. Marković, D.V. Bajuk-Bogdanović, V.B. Pavlović, A.J. Krmpot, M.M. Lekić, D.J. Jovanović, B.M. Todorović-Marković, One-step preparation of gold nanoparticles - exfoliated graphene composite by gamma irradiation at low doses for photothermal therapy applications, Materials Characterization, 173 (2021) 110944.
[15] R.S. Dey, C.R. Raj, Development of an Amperometric Cholesterol Biosensor Based on Graphene−Pt Nanoparticle Hybrid Material, The Journal of Physical Chemistry C, 114 (2010) 21427-21433.
[16] S.-K. Kim, C. Jeon, G.-H. Lee, J. Koo, S.H. Cho, S. Han, M.-H. Shin, J.-Y. Sim, S.K. Hahn, Hyaluronate–Gold Nanoparticle/Glucose Oxidase Complex for Highly Sensitive Wireless Noninvasive Glucose Sensors, ACS Applied Materials & Interfaces, 11 (2019) 37347-37356.
[17] M.N.I. Amir, A. Halilu, N.M. Julkapli, A. Ma'amor, Gold-graphene oxide nanohybrids: A review on their chemical catalysis, Journal of Industrial and Engineering Chemistry, 83 (2020) 1-13.
[18] G. Neri, E. Fazio, P.G. Mineo, A. Scala, A. Piperno, SERS Sensing Properties of New Graphene/Gold Nanocomposite, Nanomaterials, 9 (2019) 1236.
[19] H. Moustaoui, J. Saber, I. Djeddi, Q. Liu, A.T. Diallo, J. Spadavecchia, M. Lamy de la Chapelle, N. Djaker, Shape and Size Effect on Photothermal Heat Elevation of Gold Nanoparticles: Absorption Coefficient Experimental Measurement of Spherical and Urchin-Shaped Gold Nanoparticles, The Journal of Physical Chemistry C, 123 (2019) 17548-17554.
[20] E.S. Kooij, W. Ahmed, C. Hellenthal, H.J.W. Zandvliet, B. Poelsema, From nanorods to nanostars: Tuning the optical properties of gold nanoparticles, Colloids and Surfaces A: Physicochemical and Engineering Aspects, 413 (2012) 231-238.
[21] K. Park, S. Biswas, S. Kanel, D. Nepal, R.A. Vaia, Engineering the Optical Properties of Gold Nanorods: Independent Tuning of Surface Plasmon Energy, Extinction Coefficient, and Scattering Cross Section, The Journal of Physical Chemistry C, 118 (2014) 5918-5926.
[22] X. Huang, M.A. El-Sayed, Gold nanoparticles: Optical properties and implementations in cancer diagnosis and photothermal therapy, Journal of Advanced Research, 1 (2010) 13-28.
[23] B.V. Enustun, J. Turkevich, Coagulation of Colloidal Gold, Journal of the American Chemical Society, 85 (1963) 3317-3328.

[24] Y. Shang, C. Min, J. Hu, T. Wang, H. Liu, Y. Hu, Synthesis of gold nanoparticles by reduction of HAuCl4 under UV irradiation, Solid State Sciences, 15 (2013) 17-23.
[25] M.K. Abyaneh, D. Paramanik, S. Varma, S.W. Gosavi, S.K. Kulkarni, Formation of gold nanoparticles in polymethylmethacrylate by UV irradiation, Journal of Physics D: Applied Physics, 40 (2007) 3771-3779.
[26] X. Zhao, W. Wang, L. Liu, Y. Hu, Z. Xu, L. Liu, N. Wu, N. Li, Microstructure evolution of sandwich graphite oxide/interlayer-embedded Au nanoparticles induced from γ-rays for carcinoembryonic antigen biosensor, Nanotechnology, 30 (2019) 495501.
[27] S. Wang, Y. Zhang, H.-L. Ma, Q. Zhang, W. Xu, J. Peng, J. Li, Z.-Z. Yu, M. Zhai, Ionic-liquid-assisted facile synthesis of silver nanoparticle-reduced graphene oxide hybrids by gamma irradiation, Carbon, 55 (2013) 245-252.
[28] X. Li, L. Liu, Z. Xu, W. Wang, J. Shi, L. Liu, M. Jing, F. Li, X. Zhang, Gamma irradiation and microemulsion assisted synthesis of monodisperse flower-like platinum-gold nanoparticles/reduced graphene oxide nanocomposites for ultrasensitive detection of carcinoembryonic antigen, Sensors and Actuators B: Chemical, 287 (2019) 267-277.
[29] H. K, R.P. Joshi, S. D.V, V.N. Bhoraskar, S.D. Dhole, Anchoring of Ag-Au alloy nanoparticles on reduced graphene oxide sheets for the reduction of 4-nitrophenol, Applied Surface Science, 389 (2016) 1050-1055.
[30] X. Zhao, N. Li, M. Jing, Y. Zhang, W. Wang, L. Liu, Z. Xu, L. Liu, F. Li, N. Wu, Monodispersed and spherical silver nanoparticles/graphene nanocomposites from gamma-ray assisted in-situ synthesis for nitrite electrochemical sensing, Electrochimica Acta, 295 (2019) 434-443.
[31] Y. Zhang, H.-L. Ma, K. Cao, L. Wang, X. Zeng, X. Zhang, L. He, P. Liu, Z. Wang, M. Zhai, Gamma Irradiation-Induced Preparation of Graphene–Ni Nanocomposites with Efficient Electromagnetic Wave Absorption, Materials, 11 (2018) 2145.
[32] G. Baldacchino, E. Brun, I. Denden, S. Bouhadoun, R. Roux, H. Khodja, C. Sicard-Roselli, Importance of radiolytic reactions during high-LET irradiation modalities: LET effect, role of O2 and radiosensitization by nanoparticles, Cancer Nanotechnology, 10 (2019) 3.
[33] D. Kepić, S. Sandoval, Á.P.d. Pino, E. György, L. Cabana, B. Ballesteros, G. Tobias, Nanosecond Laser-Assisted Nitrogen Doping of Graphene Oxide Dispersions, ChemPhysChem, 18 (2017) 935-941.
[34] D. Long, W. Li, L. Ling, J. Miyawaki, I. Mochida, S.-H. Yoon, Preparation of Nitrogen-Doped Graphene Sheets by a Combined Chemical and Hydrothermal Reduction of Graphene Oxide, Langmuir, 26 (2010) 16096-16102.
[35] D. Li, M.B. Müller, S. Gilje, R.B. Kaner, G.G. Wallace, Processable aqueous dispersions of graphene nanosheets, Nature Nanotechnology, 3 (2008) 101-105.
[36] V. Ţucureanu, A. Matei, A.M. Avram, FTIR Spectroscopy for Carbon Family Study, Critical Reviews in Analytical Chemistry, 46 (2016) 502-520.
[37] D. Yang, A. Velamakanni, G. Bozoklu, S. Park, M. Stoller, R.D. Piner, S. Stankovich, I. Jung, D.A. Field, C.A. Ventrice, R.S. Ruoff, Chemical analysis of graphene oxide films after heat and chemical treatments by X-ray photoelectron and Micro-Raman spectroscopy, Carbon, 47 (2009) 145-152.
[38] Z. Qi, J. Shi, Z. Zhang, Y. Cao, J. Li, S. Cao, PEGylated graphene oxide-capped gold nanorods/silica nanoparticles as multifunctional drug delivery platform with enhanced near-infrared responsiveness, Materials Science and Engineering: C, 104 (2019) 109889.

[39] D.K. Roper, W. Ahn, M. Hoepfner, Microscale Heat Transfer Transduced by Surface Plasmon Resonant Gold Nanoparticles, The Journal of Physical Chemistry C, 111 (2007) 3636-3641.
[40] W. Yang, B. Xia, L. Wang, S. Ma, H. Liang, D. Wang, J. Huang, Shape Effects of Gold Nanoparticles in Photothermal Cancer Therapy, Materials Today Sustainability, 13 (2021) 100078.
[41] K. Jiang, D. A. Smith, A. Pinchuk, Size-Dependent Photothermal Conversion Efficiencies of Plasmonically Heated Gold Nanoparticles, The Journal of Physical Chemistry C, 117 (2013) 27073-27080.
[42] Z. Li, O. Johnson, J. Huang, T. Feng, C. Yang, Z. Liu, W. Chen, Enhancing the photothermal conversion efficiency of graphene oxide by doping with NaYF4: Yb, Er upconverting luminescent nanocomposites, Materials Research Bulletin 106 (2018) 365-370.
[43] Ol.A. Savchuk, J.J. Carvajal, J. Massons, M. Aguiló, F. Díaz, Determination of Photothermal Conversion Efficiency of Graphene and Graphene Oxide Through an Integrating Sphere Method, Carbon 103 (2016) 134-141.
[44] M. Hashemi, M. Omidi, B. Muralidharan, H. Smyth, M.A. Mohagheghi, J. Mohammadi, T.E. Milner, Evaluation of the Photothermal Properties of a Reduced Graphene Oxide/Arginine Nanostructure for Near-Infrared Absorption, ACS Applied Materials & Interfaces 9 (2017) 32607-32620.

- Low-dose gamma irradiation was employed to obtain gold nanoparticles anchored onto graphene oxide sheets
- Gold nanoparticles were homogeneously distributed at the graphene oxide surface and have predominately spheric shapes
- The smallest nanoparticles were reported for the dose of 1 kGy
- An increase in the irradiation dose caused either the growth of larger particles or the broad distribution of particles' sizes
- The photothermal efficiency was the highest for the sample prepared at 20 kGy

Declaration of interests

☒ The authors declare that they have no known competing financial interests or personal relationships that could have appeared to influence the work reported in this paper.

☐ The authors declare the following financial interests/personal relationships which may be considered as potential competing interests: